The Structural Basis of Calcium Dependent Inactivation of the Transient Receptor Potential Vanilloid 5 Channel

Fedir M. Bokhovchuk, Neil Bate, Nadezhda V Kovalevskaya, Benjamin T. Goult, Chris A.E.M. Spronk, and Geerten W. Vuister

Biochemistry, **Just Accepted Manuscript** • DOI: 10.1021/acs.biochem.7b01287 • Publication Date (Web): 27 Mar 2018

The Structural Basis of Calcium Dependent Inactivation of the Transient Receptor Potential Vanilloid 5 Channel

Fedir M. Bokhovchuk[1], Neil Bate[1], Nadezda V. Kovalevskaya[1,#], Benjamin T. Goult[1,&], Chris A.E.M. Spronk[1,2,‡] & Geerten W. Vuister[1,*]

[1] Department of Molecular and Cell Biology, Leicester Institute of Structural and Chemical Biology, University of Leicester, Lancaster Road, Leicester LE1 9HN, United Kingdom.

[2] JSC Spronk, Vilnius, Lithuania.

 # Present address:

Repositive Ltd, Future Business Centre, King's Hedges Road, Cambridge CB4 2HY, United Kingdom

& Present address:

School of Biosciences, University of Kent, Canterbury, Kent, CT2 7NJ, United Kingdom

‡ Chris Spronk passed away on February 28th 2018

* Corresponding author (gv29@leicester.ac.uk)

Abstract

The Transient Receptor Potential Vanilloid Channel subfamily member 5 (TRPV5) is a highly selective calcium ion channel predominately expressed in the kidney epithelium that plays an essential role in calcium reabsorption from renal infiltrate. In order to maintain Ca^{2+} homeostasis, TRPV5 possesses a tightly regulated negative feedback mechanism, where the ubiquitous Ca^{2+}-binding protein Calmodulin (CaM) directly binds to the intracellular TRPV5 C-terminus, thus regulating TRPV5. Here we report on the characterisation of the TRPV5 C-terminal CaM binding site and its interaction with CaM at an atomistic level. We have solved the *de novo* solution structure of the TRPV5 C-terminus in complex with a CaM mutant, creating conditions that mimic the cellular basal Ca^{2+} state. We demonstrate that under these conditions the TRPV5 C-terminus is exclusively bound to the CaM C-lobe only, while conferring conformational freedom to the CaM N-lobe. We also show that at elevated calcium levels, additional interactions between the TRPV5 C-terminus and CaM N-lobe occur, resulting in formation of a tight 1:1 complex, effectively making the N-lobe the calcium sensor. Together, these data are consistent with, and support the novel model for Ca^{2+}/CaM-dependent inactivation of TRPV channels as proposed by Bate et al. (Biochemistry, 2018, in press).

keywords

TRPV5 / calcium channel / NMR / structure / dynamics / calmodulin

Introduction

The Transient Receptor Potential Vanilloid subfamily member 5 (TRPV5)* is a highly-selective epithelial Ca^{2+} ion channel, predominately expressed in the apical epithelial membrane at the distal convoluted and connecting tubule of the kidney[1]. In the human kidney, approximately 95–98% of filtered Ca^{2+} is reabsorbed along renal tubules[2]. TRPV5 constitutes the apical entry gate for the transcellular reabsorption of Ca^{2+} along the tubule and thus plays a central role in reabsorption of Ca^{2+}. Gene knock-out studies showed that the ablation of TRPV5 results in a dramatic reduction of renal Ca^{2+} intake which concomitantly induces a compensatory hyperabsorption of dietary Ca^{2+} and bone abnormalities[3]. As TRPV5 is essential for the total body Ca^{2+}-homeostasis, its activity at the membrane is tightly regulated at the expression[4], trafficking[1,5] and the level of turnover[6].

When present at the plasma membrane under physiological levels of the membrane potential TRPV5 is constitutively open, resulting in a gradient-driven Ca^{2+} transport into the cell[7]. In order to be protected from the toxic influx of extracellular Ca^{2+}, electrophysiology studies demonstrated that TRPV5 employs a fast negative feedback gating mechanism, inactivating the channel upon elevated local intracellular Ca^{2+} concentration[8]. Several proteins that directly interact with TRPV5 intra-cellularly have been identified, including ones that also can bind Ca^{2+}. Examples of these are Calbindin-D28K[9], S100A10 [1], 80-KH[10] and Calmodulin (CaM) [8,11-13], where the latter was identified as a crucial factor in the Ca^{2+}-dependent inactivation of TRPV5.

Calmodulin is a highly conserved, ubiquitous Ca^{2+}- binding protein, essential as an intracellular Ca^{2+} sensor and regulator of the activity of many ion-channels in all eukaryotic cells. Functional CaM is comprised of 148 residues and has a dumbbell

* **Abbreviations** CaM: Calmodulin; C-tail: C-terminal tail of the channel; CSP: chemical shift perturbation; HSQC: heteronuclear single-quantum correlation spectroscopy; ITC: isothermal titration calorimetry; NMR: nuclear magnetic resonance; N-tail: N-terminal tail of the channel; TRP: transient receptor potential; TRPV: transient receptor potential vanilloid; $TRPV5^{655-725}$: transient receptor potential vanilloid 5 residues 655-725.

shaped structure formed by two domains, or lobes (subsequently denoted as the N-lobe and C-lobe), which are connected by a flexible linker region[14,15].

For TRPV5, it was shown that the truncation of thirty of its C-terminal residues dramatically diminished Ca^{2+}-dependent inactivation of the channel[16]. In silico prediction followed by subsequent biophysical characterization identified five putative CaM binding sites in the TRPV5 N- and C-terminal tails[13]. The most distal of these CaM binding regions at the C-terminus was shown crucial, as point mutants lacking CaM binding exhibited reduced Ca^{2+}-dependent inactivation[12]. The closely related TRPV6 channel displayed a similar dependancy on CaM binding to the analogous region at its C-terminus[17]. Other members of the TRP family, i.e. for TRPC1 [18], TRPV1 [19], and TRPV4 [20], also showed a desensitization of the Ca^{2+}-dependent negative feedback mechanism upon truncation of their C-terminal CaM binding sites. For TRPV2, CaM was shown to directly bind the intracellular C-terminus[21]. Taken together, these studies indicate that for TRPV5, binding of CaM to the C-terminal binding site is essential for the fast Ca^{2+}-dependent inactivation of the channel. However, the molecular mechanism(s) by which CaM interacts with the TRPV5 terminus and exerts its inactivating mechanism remains unclear.

Atomic resolution structures of the N-terminal and membrane-spanning parts of the TRPV1 [22], TRPV2 [23], TRPV5 [24] and TRPV6 [25,26] channels have confirmed the predicted tetrameric assembly of the TRPV channels in analogy of the potassium and calcium ion channels. The structures have yielded invaluable knowledge on the ion-binding sites, pore structure, the location of the N-terminal Ankyrin repeat domains and the rearrangements of the membrane-spanning moieties leading to channel closure. However, in all structures the C-terminal parts of the channels were either omitted from the expression vectors or no data was obtained. Thus, the calcium-dependent regulation by CaM remains enigmatic.

Recently, Bate et al.[27] proposed a novel three-step regulatory model for TRPV6 inactivation by CaM. According to this model, at basal intracellular Ca^{2+} levels the TRPV6 C-terminus could be constitutively bound to the CaM C-lobe. Upon elevated Ca^{2+}, additional interactions between the TRPV6 C-terminus and CaM N-lobe occur, which leads to a CaM-TRPV6 complex in which CaM bridges two TRPV6 channel C-

termini, resulting in the formation of the inactivated form of the channel. Considering the high level of homology between TRPV5 and TRPV6, as well as the similar topology of their C-terminal CaM binding sites, it can be argued that both channels share similar modes of Ca^{2+}-dependent regulation.

The aim of the present work is to establish the structural organization of the CaM:TRPV5 complex at different Ca^{2+} conditions and thus, to suggest a mechanistic basis for the Ca^{2+}-dependent channel inactivation. Therefore, we employed high-resolution analytical gel filtration and NMR spectroscopy on various CaM-TRPV5 complexes to study the interaction at an atomistic level. We present the solution structure of the CaM-TRPV5 complex in a low-calcium mimicking state and establish how its dynamic behaviour relates to the high-calcium state leading to channel inactivation.

Materials and Methods

Protein expression and purification

The C-terminal fragment $TRPV5^{655-725}$ was amplified by PCR and inserted into the *E.coli* expression vector, pLEICS-46, which contains a 58-amino acid GB1 solubility tag and a His_6 affinity tag followed by a TEV cleavage site (Protex, University of Leicester). CaM wild-type and CaM mutants defunct in calcium binding to the N-lobe, C-lobe or both lobes, denoted as CaM_{12}, CaM_{34} and CaM_{1234} respectively[28], were amplified by PCR and inserted into the *E.coli* expression vector, pLEICS-01, which contains a His_6 affinity tag followed by a TEV cleavage site (Protex, University of Leicester). All constructs were sequence verified. Plasmids were expressed in *E.coli* BL21 Star (DE3) (Life Technologies, USA) grown in either LB, or in 2M9 minimal media for the production of unlabelled, ^{15}N- or $^{15}N/^{13}C$-labelled samples for NMR experiments. Cultures were grown at 37 °C to an OD_{600} of approximately 0.8 and induced with IPTG to a final concentration of 200 μM for CaM and 40 μM for TRPV5, and incubated overnight at 18 °C. Cells were harvested and the pellet resuspended in buffer containing 20 mM Tris-Cl pH 8.0, 50 mM imidazole, 500 mM NaCl and protease inhibitors (Protease Inhibitor Cocktail Set III,

Calbiochem). Cell disruption was achieved via sonication and the cleared lysate applied to a HisTrap™ HP column (GE Healthcare). Recombinant proteins were eluted with an imidazole gradient of 0.05-0.5 M, dialysed into 20 mM Tris-Cl pH 8.0, 50 mM NaCl, 1 mM DTT and concomitantly cleaved with TEV protease to remove N-terminal tags; GB1-His_6- (pLEICS-46) and His_6- (pLEICS-01). Cleaved recombinant proteins were further purified via anion exchange using a HiTrap™ Q HP column (GE Healthcare) and eluted with a NaCl gradient of 0.05-1 M. Recombinant proteins were analysed by 16% SDS-PAGE and stained using Coomassie brilliant blue R-250. Protein concentrations were determined from the UV absorbance at 280 nm, A_{280} (Eppendorf BioPhotometer plus) using the extinction coefficients $\varepsilon(CaM_{WT/12})$=2980 $M^{-1}cm^{-1}$, $\varepsilon(TRPV5^{655-725})$=5500 $M^{-1}cm^{-1}$ as determined by the ProtParam Tool (http://web.expasy.org/protparam).

Analytical gel filtration

Recombinant CaM and TRPV6 proteins were dialysed into gel filtration buffer (20 mM Tris-Cl pH 8.0, 150 mM NaCl and 2 mM DTT). Complexes were formed in the presence of 10 mM Ca^{2+} at room temperature for 30 minutes. Analytical gel filtration chromatography was carried out using a Superdex75 (10/300) column (GE Healthcare) pre-equilibrated and then run in gel filtration buffer.

NMR spectroscopy and sample preparation

The CaM:peptide complex under a low [Ca^{2+}] (100-300 nM) was achieved by repeated dialysis: first against 20 mM Tris-Cl pH 7.4, 2 mM EGTA pH 8.0, and subsequently against 20 mM Tris-Cl pH 7.4. The effective [Ca^{2+}] was estimated on the basis of ionic composition listed by the manufacturer of our chemicals used for preparation of the buffer. All other CaM:TRPV5 complexes were prepared using the following steps: FPLC Q-column CaM and TRPV5 protein fractions were separately dialyzed against NMR buffer (20 mM Tris pH 7.4, 50 mM KCl, 10 mM $CaCl_2$); the concentration was determined and components mixed at the required ratio; protein complees were concentrated using a 3.5 kDa molecular weight cut-off centricon

filter (Millipore, USA). CaM_E and the CaM_E:TRPV5 co-expression complex were dialyzed against (pH 7.4, 60 mM KCl, 20 mM Tris). All NMR samples contained 5% v/v D_2O.

NMR spectra recording, processing and assignment

The NMR spectra were recorded at 35 °C on Bruker 500 MHz AVI, 600 MHz AVIII, 600 MHz AVIII HD, or 800 MHz AVII spectrometers; the 600 MHz and 800 MHz spectrometers were equipped with CryoProbes. NMR data processing and analysis were performed using the NMRPipe[29], TOPSPIN v3.1 and CcpNmr Analysis[30] and AnalysisAssign[31] software. Non-uniformly sampled 3D and 4D spectra were reconstructed using the istHMS software[32].

The binding of TRPV5 to CaM was monitored by 2D ^{15}N-^{1}H-HSQC experiments. The previously published assignment of CaM (BMRB entry 547) was used as a starting point. For the near complete assignment of the backbone atoms of the different CaM:TRPV5 complexes, the following series of heteronuclear triple-resonance experiments were performed: 3D HNCA, HNCACB, HN(CO)CA, CBCA(CO)NH, HNCO for the unbound ^{13}C-^{15}N-CaM_{WT} and ^{13}C-^{15}N-CaM_{12} and the following complexes (Supplementary Tables 1.1 and 1.2): ^{13}C-^{15}N-CaM_{WT}:$TRPV5^{655-725}$ (1:1), ^{13}C-^{15}N-CaM_{WT}:$TRPV5^{655-725}$ (1:2), ^{15}N-CaM_{WT}:^{13}C-^{15}N-$TRPV5^{655-725}$ (1:1) and CaM_{12}:^{13}C-^{15}N-$TRPV5^{655-725}$ (1:1). CaM chemical shifts differences resulting from binding were calculated for each individual backbone amide peak as

$$\triangle\delta = \sqrt{(\triangle\delta_H)^2 + 0.15(\triangle\delta_N)^2} \qquad (1)$$

where $\Delta\delta_H$ and $\Delta\delta_N$ are the chemical shift differences for ^{1}H and ^{15}N, respectively. In order to assign peaks from disordered region of the TRPV5 moiety of the complex, direct ^{13}C-detected experiments were employed[33,34]. Side-chain atoms were assigned by comparison of the strips of the 3D ^{13}C (H)CCH/H(C)CH-TOCSY[35] spectra, recorded on Bruker 600 MHz AVIII and 600 MHz AVIII HD spectrometers, and a constant time ^{13}C-HSQC spectrum. Two-dimensional CBHD/CB(HD)HE[36] spectra

were used in order to unambiguously link β-carbon and aromatic protons of the CaM_{12} aromatic residues.

^{15}N-relaxation experiments

^{15}N-T_1, ^{15}N-T_2 and heteronuclear ^{1}H-^{15}N-NOE data were collected at 35 °C at 14.1 T (and 18.8 T as a control) using standard pulse sequences. Eight data points were measured for both T_1 and T_2, with the range of delays between 8 to 1120 ms and 4.6 to 110.4 ms, respectively, in randomized order. In the heteronuclear NOE experiment, a relaxation delay of 2.9 s was used prior to each scan. Residues with peaks overlapping in the ^{15}N-HSQC spectra were excluded from the relaxation analysis. T_1 and T_2 data were fitted using the nLinLS and expFit modules of the NMRPipe software package[29]. Intensities were subsequently fitted to an exponent using the modelXY module in NMRPipe and rates obtained. Errors of the rates were estimated using Monte-Carlo simulations from the errors of the measured peak intensities. The local rotational correlation time, (τ_c), for each individual amide group was calculated from the T_2/T_1 ratio according to Fushman et al.[37].

Structure calculation and validation

NMR NOESY spectra for aliphatic and aromatic regions were recorded at 35 °C on a Bruker 800 MHz AVII spectrometer. The NOE-mixing time was set to 80 ms in all NOESY experiments. The structures were calculated, refined and validated using the CcpNMR Analysis pipeline using CYANA3.97 [38] as described by Skinner et al.[39]. For the structure determination, the NOESY cross peaks were automatically picked and integrated by CcpNMR Analysis and then manually checked for artefacts and genuinely missed peaks by comparison of the ^{13}C-NOESY strips with the corresponding strip of the ^{13}C-TOCSY spectra. The complex was treated as a single chain in CYANA3.97, with CaM_{12} and TRPV5$^{655-725}$ sequences connected by the lengthy sequence of linker residues. Also, two Ca^{2+} ions were added to the sequence and linked to the side-chain carboxylates or carbonyls of the Asp and Glu residues 93, 95, 97, 104 and 129, 131, 133, 140 from the C-lobe EF-domains 3 and 4, respectively. The input data for CYANA consisted of the table of chemical shifts,

unassigned peaks (positions and volumes) of the NOESY spectra, backbone dihedral restraints for both moieties of the complex, as predicted from the chemical shifts values by the programs TALOS+ [40] and DANGLE[41], the list of unambiguous inter-chain distance restraints, which was obtained by manual assignment of the reciprocal CaM_{12} and $TRPV5^{655-725}$ NOESY peaks and set to 5.5 Å, and the list of lower- and upper limit distance restraints for the Ca^{2+} ion coordinate bonds, which were set to 2 Å and 3 Å, respectively.

The NOESY peaks lists were automatically assigned during seven cycles of automated assignment and structure calculation using CYANA/CANDID protocol. In each cycle, 120 structures were generated and energy minimized using 15,000 simulations steps. The NOESY spectra parameters were calibrated in the first cycle. Quality of the calculated structural NMR ensemble was analysed and validated with the CING suite available at the iCing webserver (https://nmr.le.ac.uk)[42]. The 20 lowest energy conformers were subsequently subjected to a final round of refinement using YASARA[43] in two stages. In the first stage, the CYANA structures were subjected to refinement in explicit solvent using a regular flat bottom harmonic well restraints potential with the upper limits from the CYANA consensus restraints. The resulting refined ensemble was then used in combination with the peak volumes to calibrate Log Normal target distances according to the method, suggested by Bardiaux et al.[44]. In the second stage these target distances were used for further explicit solvent refinement of the structures using log-normal potentials[45]. A table of structure quality metrics, based on the iCing report was assembled as recommended by the wwPDB NMR Validation Task Force[46].

Results

Previously, we probed the minimal TRPV5 binding sites using short peptides[13]. Here, we employed the longest soluble TRPV5 C-terminal construct residues 655-725, denoted as $TRPV5^{655-725}$ [47], to examine its interactions with CaM. Comparison of the ^{15}N-HSQC spectra of the CaM_{wt} complex of the longer 655-725 construct used in this study with the complex of the short peptide used previously,

shows notable differences (Fig. S1A), suggesting additional effects caused by residues outside the previously postulated binding region. Also, for the paralogue TRPV6 it was established that the flanking residues were crucial in CaM-dependent inactivation[27]. Consequently, this renders our current, longer construct a better model for studying the CaM-TRPV5 interaction.

We first set out to establish the nature of the CaM-TRPV5 interaction under low [Ca^{2+}]. Both N- and C- CaM lobes contain two EF hands (helix-loop-helix motifs) that together can bind up to four Ca^{2+} ions per molecule of CaM[15]. Despite the high sequence similarity of the two globular domains, it was shown *in vitro* that Ca^{2+} ions binds to the CaM C-lobe with a positive cooperativity and individual macroscopic equilibrium dissociation constants (K_d) between 25 and 200 nM, whereas approximately 6 times lower affinity for the N-lobe was reported[48]. Consequently, given that the resting cytosolic concentrations of free Ca^{2+} in the epithelial cells is about 100 nM[49], the CaM C-lobe is expected to be at least partially Ca^{2+} loaded at basal conditions, whereas the N-lobe is fully Ca^{2+}-loaded only under conditions of significant calcium influx. In order to investigate the interactions of TRPV5 and CaM under representative basal cellular conditions, we purified ^{15}N-CaM_{WT} from *E.coli* where neither exogenous Ca^{2+}, nor Ca^{2+}-chelating agents were added during protein purification (denoted as CaM_E). The ^{15}N-HSQC spectrum of CaM_E reveals that it exists as a heterogeneous mixture under these conditions, that can be readily resolved by the subsequent addition of excess Ca^{2+} (Figs S2A-C). In accordance with the ~6 fold higher affinity of the CaM C-lobe for Ca^{2+} compared to the N-lobe, the spectra show that Ca^{2+} binds initially to the CaM C-lobe predominantly, followed by binding of Ca^{2+} into the N-lobe. Moreover, only 2.5 equivalents of Ca^{2+} are required to convert one CaM_E to a fully Ca^{2+}-loaded state (Fig. S2C, compare with Fig. S2B), showing that each CaM_E moiety is on-average loaded with ~1 Ca^{2+} ion. Since the intracellular concentration of free Ca^{2+} in *E.coli* is ~90 nM[50], which is approximately the same as determined for renal epithelial cells[49], we believe CaM_E to be a good representative of resting free intracellular CaM.

Next, as a proxy for complex formation under cellular conditions we used a transcriptional fusion to co-express His_6-CaM and a tag-less $TRPV5^{655-725}$ C-tail in

E.coli. We co-purified a ^{15}N-CaM$_E$ / ^{15}N-CaM$_E$ -^{15}N-TRPV5$^{655-725}$ mixture using the His$_6$ tag attached to CaM, again without addition of exogenous Ca^{2+} or Ca^{2+}-chelating agents, and examined this sample response to increasing [Ca^{2+}] using ^{15}N-HSQC experiments (Fig. 1 and Figs S2D-H). The spectra showed that the sample comprised a heterogeneous mixture of both free CaM$_E$ and CaM$_E$ bound to TRPV5, which displayed a differential behaviour upon addition of exogenous Ca^{2+} (Fig. 1A). We used the relative intensities of representative cross-peaks as a proxy for the presence and/or dynamic exchange of Ca^{2+} in these different states. The signals from the CaM$_E$ C-lobe in complex with TRPV5$^{655-725}$ are unaffected by increasing [Ca^{2+}] (Fig. 1B), indicating that the C-lobe has effectively sequestered Ca^{2+} in both its Ca^{2+}-binding sites. In contrast, the signals of free, i.e. non-complexed, CaM$_E$ C-lobe show a steady increase in intensity (Fig. 1C), with its maximum reached after the addition of 3 equivalents of Ca^{2+}, similar to that previously seen for CaM$_E$ in isolation. Hence, the behaviour of CaM$_E$ under resting cellular [Ca^{2+}] is very different depending on whether it is in complex with TRPV5$^{655-725}$. In the absence of TRPV5$^{655-725}$, CaM$_E$ exists in a mixture of calcium bound states; however, the presence of TRPV5$^{655-725}$ stabilises the fully Ca^{2+}-loaded C-lobe. Therefore, we conclude that at basal conditions the tail of the TRPV5 channel can be bound to a fully Ca^{2+}-loaded C-lobe.

To test our ability to reproduce these results under *in vitro* conditions we first generated CaM$_{WT}$:TRPV5$^{697-712}$ complexes at fully-apo, basal and elevated intracellular Ca^{2+} concentrations and recorded ^{15}N-HSQC spectra (Figs 1D,E). Careful comparison of these spectra shows that under basal cytosolic Ca^{2+} concentration, the CaM$_{WT}$ C-lobe again appears in a Ca^{2+}-loaded and bound state, whereas the data are consistent with an N-lobe devoid of Ca^{2+} or TRPV5 interaction.

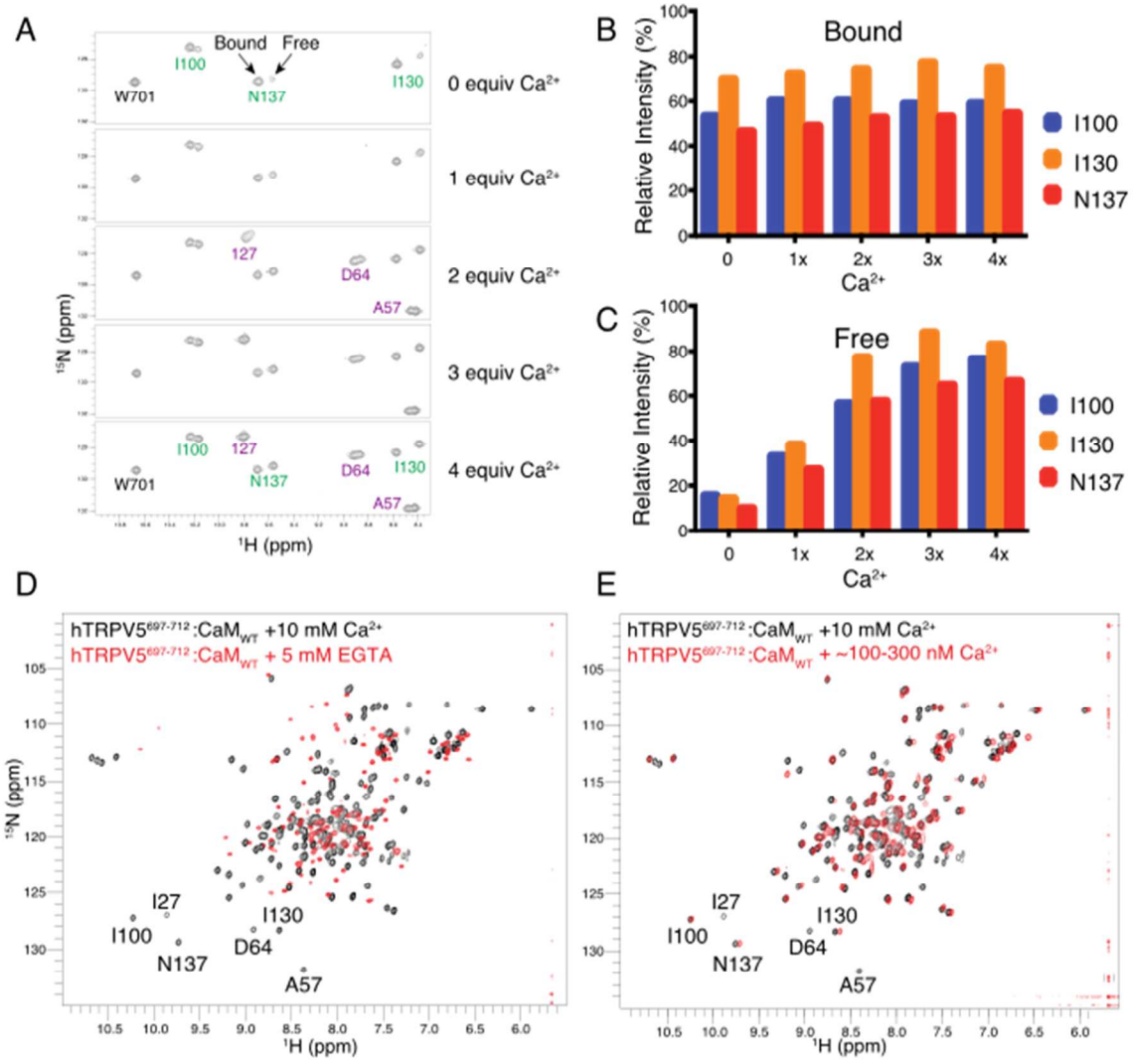

Figure 1. Calmodulin is bound via its C-lobe to the TRPV5 C-tail under low Ca^{2+} conditions.

(**A**) Small regions of the ^{15}N-^{1}H-HSQC spectra of ^{15}N-labelled CaM and ^{15}N-labeled $TRPV5^{655-725}$, which were co-expressed in *E.coli* and purified in the absence of exogenous Ca^{2+}, at increasing Ca^{2+}-stoichiometries. Selected residues are indicated. Full spectra displayed in Figs S2(**D-H**); (**B, C**) Comparison of the relative peak intensities for different residues in (B) bound and (C) free states, derived from the spectra displayed in (A) using TRPV5 residue W701 as calibration reference; (**D**) ^{15}N-HSQC spectra of CaM_{WT} in complex with 2x amount of $TRPV5^{697-712}$ upon addition of 10 mM $CaCl_2$ (black) and 5mM EGTA (red); (**E**) ^{15}N-HSQC spectra of CaM_{WT} in complex with 2x amount of $TRPV5^{697-712}$ upon addition of 10 mM $CaCl_2$ (black) and with residual amounts of Ca^{2+} (no Ca^{2+} added during purification/sample preparation; see methods) (red).

In order to study the larger and more representative CaM:TRPV5$^{655-725}$ complex at low Ca^{2+} concentration in a highly controlled and reproducible fashion, for NMR experiments we employed a previously described E32Q/E68Q N-lobe double mutant, denoted as CaM_{12}, which prevents the N-lobe from binding Ca^{2+} while retaining the full Ca^{2+} binding capacity for the C-lobe[28]. First, binding of this N-lobe functional mutant to TRPV5$^{655-725}$ was studied by analytical gel-filtration at high-Ca^{2+} conditions along with the CaM_{34} and CaM_{1234} mutants, where the Ca^{2+}-binding sites are mutated in the C-lobe or in both lobes, respectively. Similar to the corresponding TRPV6 region[27], the formation of the stable complex was observed by gel filtration only for CaM_{12}:TRPV5$^{655-725}$ (Fig. S3A), whereas no evidence of interaction was found for CaM_{34} (Fig. S3B) or CaM_{1234} (Fig. S3C). Systematic comparisons of the NMR data collected for the CaM_{WT}:TRPV5$^{697-712}$ complexes under various [Ca^{2+}] and the CaM_{12}:TRPV5$^{655-72}$ complex (cf. compare Fig. S1B and Fig. 1E) indicates the latter to be a valid model for the CaM:TRPV5 complex at the basal calcium state.

CaM:TRPV5$^{655-725}$ interaction at different Ca^{2+} conditions

To identify CaM amino acids involved in the interaction with TRPV5, changes in ^{1}H-^{15}N cross-peak positions in response to varying concentrations of TRPV5 were monitored. 2D ^{1}H-^{15}N HSQC spectra of ^{15}N-CaM_{12} and ^{15}N-CaM_{wt} in the ligand-free apo-state and upon addition of an equimolar, and 2-fold excess of unlabelled TRPV5$^{655-725}$ were collected, overlaid and analysed. This analysis revealed significant differences in patterns of the perturbations of the peaks of distinct N- and C-lobe amino acids upon binding (Figs 2A,B). In order to investigate this interaction for the whole CaM backbone, conventional heteronuclear multi-dimensional triple-resonance NMR methods were utilized to assign the ^{1}H, ^{15}N and ^{13}C backbone resonances of CaM_{wt} and CaM_{12} as 1:1 and 1:2 complexes with unlabelled TRPV5$^{655-725}$ along with apo-^{15}N-CaM_{12}. Overall, more than 95% of backbone resonances were unambiguously assigned for all complexes, excluding Prolines 43 and 66, and Ser 81 from the flexible linker connecting the CaM N- and C-

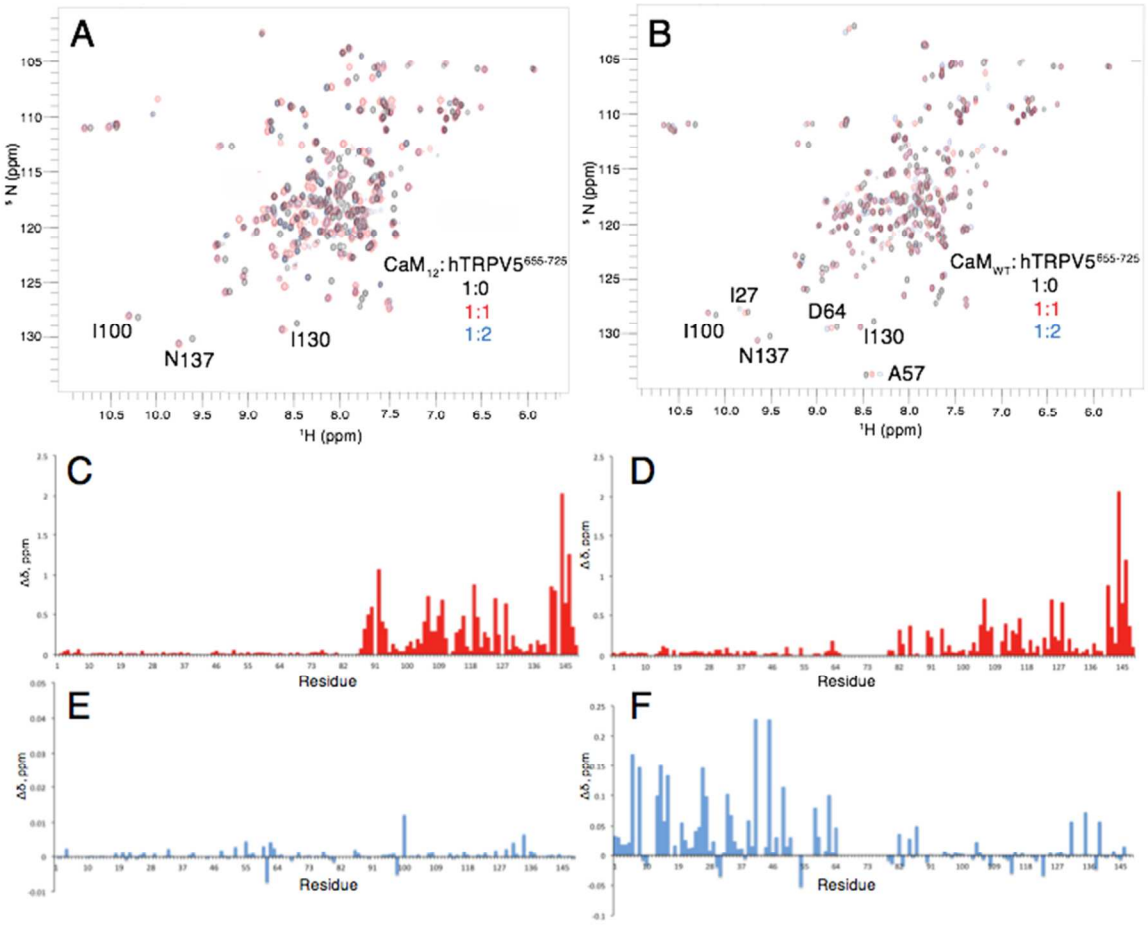

Figure 2. NMR data of the CaM$_{12}$:TRPV5$^{655-725}$ and CaM$_{WT}$:TRPV5$^{655-725}$ complexes. (**A**) ^{15}N-^{1}H-HSQC spectra of CaM$_{12}$ upon addition of 0.0 (black), 1.0 (red), 2.0 (blue) molar equivalent of TRPV5$^{655-725}$. Note that the blue 1:2 peaks are overlapping within the linewidth and hence near invisible; (**B**) ^{15}N-^{1}H-HSQC spectra of CaM$_{WT}$ upon addition of TRPV5$^{655-725}$, stoichiometries and color coding identical to (**A**); (**C**) ^{1}H-^{15}N-CSP analysis of CaM$_{12}$ upon binding of TRPV5$^{655-725}$ (1:1 complex vs. unbound); (**D**) ^{1}H-^{15}N-CSP analysis of CaM$_{WT}$ upon binding of TRPV5$^{655-725}$ (1:1 complex vs. unbound); **(E)** ^{1}H-^{15}N-CSP analysis of CaM$_{12}$ upon binding of TRPV5$^{655-725}$ (1:2 complex vs. 1:1 complex); Note that the scale is 5 times smaller as compared to the scale of (**F**) and all effects fall within the margin of error; **(F)** ^{1}H-^{15}N-CSP analysis of CaM$_{WT}$ upon binding of TRPV5$^{655-725}$ (1:2 complex vs. 1:1 complex).

domains. Analysis of the residue-specific chemical shift perturbations (CSP) (δ_{bound}-δ_{free}) as a function of residue number demonstrates the lobe-specificity of CaM:TRPV5 interaction (Figs 2C-F). Upon addition of equimolar amount of TRPV5$^{655-725}$ to both CaM$_{12}$ and CaM$_{wt}$ the largest perturbations are observed for the C-lobe residues (Figs 2C,D), with negligible effects on the CaM$_{12}$ N-lobe and small,

but relevant perturbations for the CaM_{WT} N-lobe. Remarkably, the magnitudes of the C-lobe perturbations are very similar for CaM_{12} and CaM_{WT}, with the very large shifts observed for residues Phe92, Ala128 and Met144, which are located in the hydrophobic binding-pocket of the CaM C-lobe[51]. In contrast, upon addition of an excess amount of TRPV5, an additional set of perturbations was observed only for the residues from the Ca^{2+}-loaded N-lobe of CaM_{WT}, with no observable effects for the N-lobe of CaM_{12} (Figs 2E,F). These CSP data illustrate the asymmetry in the interaction of TRPV5 with the CaM N- and C-domains and provide strong evidence that the formation of the complex between the CaM C-lobe and TRPV5 C-terminus plays a central role in the TRPV5 inactivation mechanism.

Structure of the CaM_{12}:$TRPV5^{655-725}$ complex

We aimed to establish the atomic basis of the TRPV5-CaM interaction under low Ca^{2+} conditions, and therefore set out to solve the structure of the CaM_{12}:$TRPV5^{655-725}$ complex by high-resolution solution NMR spectroscopy. To assign the side-chain resonances, H(C)CH- and (H)CCH-TOCSY and ^{13}C-NOESY spectra were collected for the complex and analysed in combination. Resonance assignments were achieved for 95% of side-chain atoms from the CaM_{12} moiety of the complex (Fig. S4A).

In-silico order predictions for TRPV5 by the PONDR server[52] suggests that the TRPV5 cytoplasmic sequence is predominately intrinsically disordered, with only the $TRPV5^{700-708}$ region predicted to be α-helical (Fig. S4B). Indeed, triple-resonance data recorded for ^{13}C/^{15}N-labelled $TRPV5^{655-725}$ in complex with unlabelled CaM, yielded data indicative of wildly varying motional regimes often compromising spectral quality (not shown). However, by combining direct ^{13}C-detected and conventional heteronuclear methods for the CaM_{12}:^{13}C-^{15}N-$TRPV5^{655-725}$ sample, 100% of backbone and 87% of side-chain resonances were assigned for the structured region. Overall, 52% of the backbone and 42% of the side-chain proton resonances were assigned for the full TPRV5 moiety of the complex.

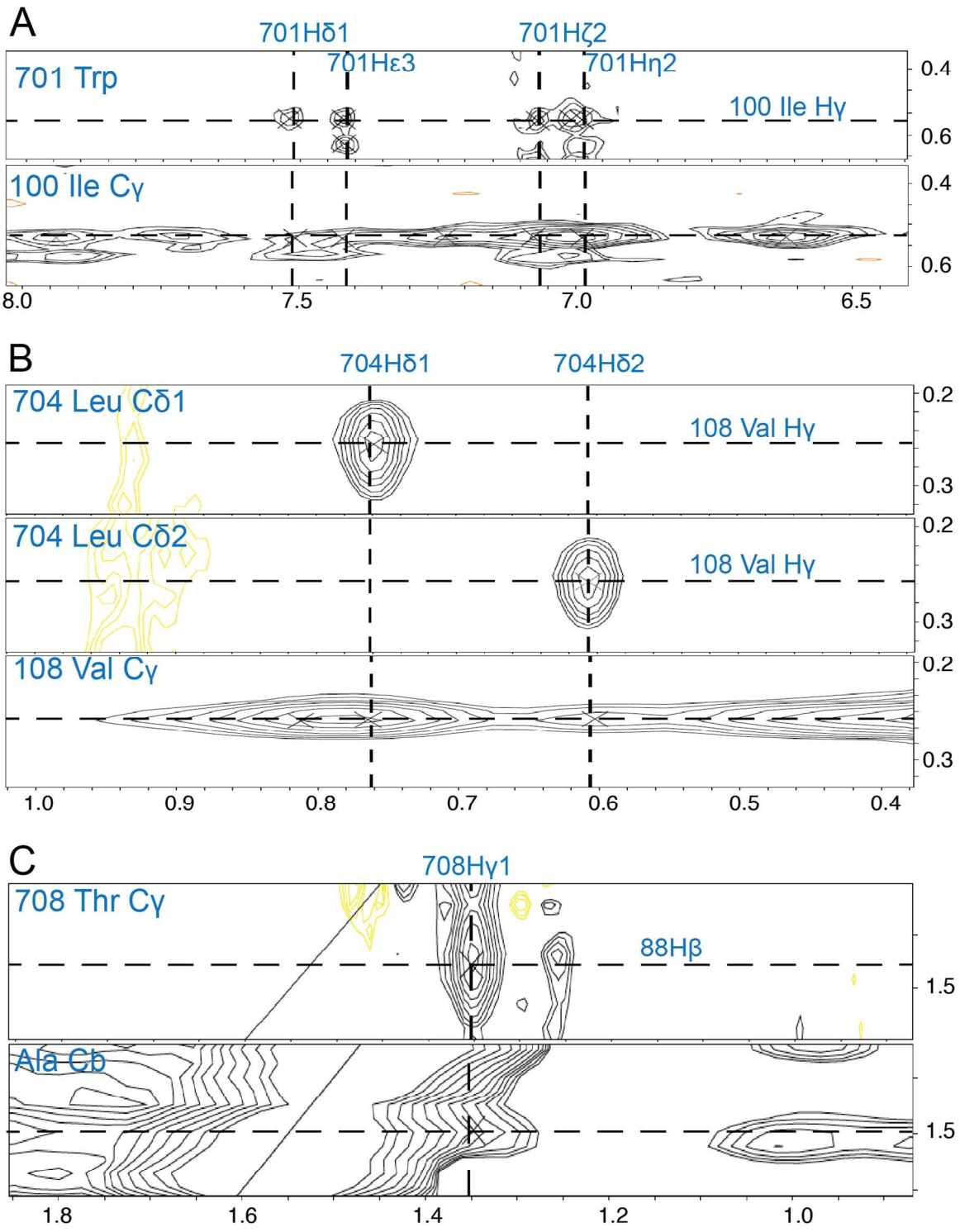

Figure 3. Selected strips of ^{13}C-NOESY spectra of the CaM$_{12}$:TRPV5$^{655-725}$ complex. The strips display unambiguously assigned intermolecular NOEs between TRPV$^{655-725}$ and CaM$_{12}$. (**A**) Matched strips showing the NOEs between the indole ring protons of Trp701 and the methyl groups of Ile100; (**B**) Matched strips showing the NOEs between the methyl groups of Leu704 and Val108; (**C**) Matched strips showing the NOEs between the methyl groups of Thr708 and Ala88. Horizontal dotted lines indicate proton assignments for the CaM$_{12}$ atoms, vertical dotted lines correspond to the assignments of the matching TRPV5$^{655-725}$ protons, crosses indicate the centre of the peak.

In order to obtain the NOE distance restraints within and between the two chains of the complex, a series of 3D and 4D NOESY experiments (see Table S1) were collected and analysed for the different samples with different selectively isotope-labelled moieties of the complex. Individual NOE strips of 3D ^{13}C-NOESY and ^{15}N-NOESY spectra, collected on the different samples, were manually inspected and cross-peaks consistent with intermolecular NOEs were identified. Interestingly, and in contrast to the expectations derived on the basis of the CaM-TRPV1 complex[53], neither intermolecular NOEs between TRPV5$^{655-725}$ and the CaM N-lobe residues, nor long-range intermolecular NOEs between the CaM N- and C-lobes residues were observed, indicating the absence of any intramolecular contacts between the C- and N-lobes of CaM. In contrast, numerous intermolecular NOEs between the CaM C-lobe and the helical region of TRPV5$^{655-725}$ were identified in the ^{13}C-NOESY spectra (Fig. 3). The ^{13}C-aromatic-NOESY spectrum displayed characteristic NOE cross peaks between Trp701 and the methyl groups of CaM$_{12}$ Ile100 (Fig. 3A). The symmetric NOE was also observed at the Ile100 Cγ strip in the ^{13}C-NOESY-HSQC experiment (Fig. 3A), collected for the reciprocally labeled sample 1 (see Table S2.1). Similarly, NOEs were also observed between the TRPV5 Trp701 and other hydrophobic C-lobe residues, namely Ala128 and Met144. In accordance, these CaM$_{12}$ residues demonstrate the highest CSP values upon binding of TRPV5$^{655-725}$ (Fig. 2C). Trp701 was previously identified as a key residue for the interaction[13,54], and the observation of multiple intramolecular NOEs confirms that Trp701 anchors the TRPV5 C-terminal helix to the hydrophobic pocket of the CaM C-domain. Similarly, symmetric NOEs were also observed for Leu704, interacting with Phe92, Val108 (Fig. 3B), Met109, and Phe141. In addition, intermolecular NOEs were found between the Methyl-protons of residues Ala88 and Val108 of CaM$_{12}$ and TRPV5 residue Thr708, flanking the predicted helical region of TRPV5$^{655-725}$ (Fig. 3C).

The list of 16 upper limit restraints, derived from these unambiguously assigned intermolecular NOEs, together with a set of 268 dihedral angles restraints, generated using both TALOS+ and DANGLE software packages, and the otherwise unassigned NOESY peaklists were used in structure calculations, performed with

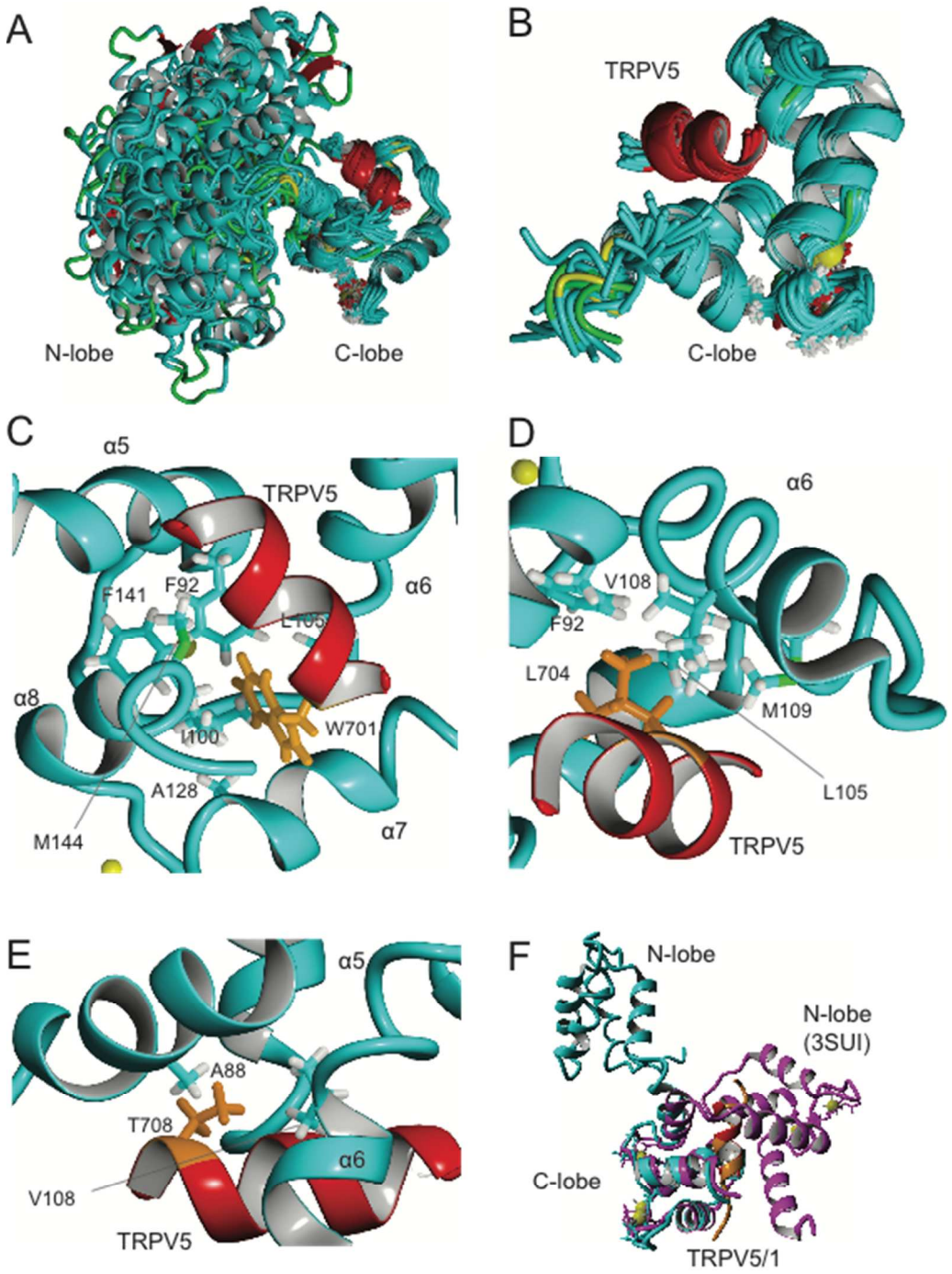

Figure 4. Structure of the CaM_{12}:$TRPV5^{655\text{-}725}$ complex.

(**A,B**) CaM C-lobe and $TRPV^{700\text{-}708}$ best-fit backbone superposition of the 20 refined structures calculated for the complex, with N-lobe shown (**A**) and hidden (**B**). The $TRPV5^{700\text{-}709}$ helix is colored red, CaM_{12} is colored cyan; (**C-E**) Zoomed views, highlighting the surrounding side-chains of CaM_{12} residues with detected NOE contacts as sticks, for Trp701, Leu704, and Thr708, respectively (orange); (**F**) Superimposed C-lobes of representative member of the CaM_{12}:$TRPV5^{655\text{-}725}$ ensemble (cyan) and CaM in complex with the TRPV1 peptide (PDB id 3SUI; purple). The TRPV1 peptide (orange) and residues 700-709 of TRPV5 (red) are tightly overlapping.

CYANA/CANDID[38]. The program automatically generated 1804 unique NOE distance restraints from the available peaks (Table 1), with 119 of the 394 long-range NOEs identified as inter-chain NOEs. No inter-chain NOEs were observed for the residues located beyond the α-helical region TRPV5$^{700\text{-}708}$ and the C-lobe region CaM$_{12}$$^{74\text{-}148}$.

Figure 4A shows the ensemble of the 20 lowest-energy structures calculated for the CaM$_{12}$:TRPV5$^{655\text{-}725}$ complex after seven rounds of CYANA calculations followed by a water refinement protocol (see Methods) aligned on the C-lobe. These structures were assessed for the absence of upper distance NOE violations > 0.5 Å, and absence of dihedral angle violations > 5° after their initial CYANA calculations and demonstrated good convergence with an acceptable pairwise rmsd value of <1.2 Å for the backbone atoms in the regions CaM$_{12}$$^{78\text{-}148}$ and TRPV5$^{700\text{-}708}$ (see Table 1 for structure calculation statistics). In accordance with the previously discussed NOE data, no contacts were found between the CaM$_{12}$ N-lobe and TRPV$^{655\text{-}725}$ or CaM C-lobe, resulting in adoption of scattered conformations of the N-lobe with respect to the C-lobe (Fig. 4A). Predictably, the absence of inter-molecular restraints between the N-lobe and TRPV5$^{655\text{-}725}$, leads to significantly higher values of the pairwise mean square deviation in the ensemble for the CaM$_{12}$ N-lobe residues, with respect to the C-lobe residues (2.1 Å vs. 1.2 Å, respectively).

The structure of the complex shows that CaM$_{12}$ interacts with TRPV$^{655\text{-}725}$ through its C-lobe in an anti-parallel mode, with TRPV residues Gly700-Leu709 in a helical conformation and a topology similar to those reported for other CaM complexes, such as those with the Munc peptide[55] or the HIV-1 Matrix protein[56]. The major stabilizing factor for the interaction between the CaM C-lobe and TRPV$^{700\text{-}709}$ is the deep anchoring of the Trp701 and Leu704 side chains into the C-terminal hydrophobic pocket of CaM (Figs 4C,D). In accordance with numerous NOE cross-peaks, the indole ring of the Trp701 is in close proximity to residues Phe92, Ile100, Leu105, Ala128, Phe141 and Met144 (Fig. 4C). The methyl groups of Leu704 in the centre of the helix interact with the side chains of CaM$_{12}$ residues Phe92, Leu105, Val108 and Met109. The third key residue Thr708, located at the C-terminal end of the structured TRPV5$^{655\text{-}725}$ region, is inserted deep into the hydrophobic cleft between the helixes α5 and α6 of CaM$_{12}$, where it contacts residues Ala88 and

Val108 and thus, determines the orientation of the TRPV5 helix along the CaM_{12} helix α5 (Fig. 4E). Interestingly, the side-chain of Arg705 is packed between the side-chains of residues Met144 and Met145.

Table 1. Structural statistics

Completeness of resonance assignments	
Backbone	96% (CaM_{12}) 100 % ($TRPV5^{700-708}$)
Side chain	95% (CaM_{12}) 87% ($TRPV5^{700-708}$)
Aromatic	88% (CaM_{12}) 90% ($TRPV5^{700-708}$)
Stereospecific methyl	0%
Conformationally restricting restraints	
Distance restraints	
Total	1803
Intraresidue (i = j)	578
Sequential (|i-j| = 1)	485
Medium range (1 < |i-j| < 5)	346
Long range (|i-j|≥ 5)	394
Inter-monomer (between CaM_{12} and $TRPV5^{655-725}$)	119
Dihedral angle restraints	268
Hydrogen-bond restraints	0
Disulfide restraints	0
Number of restraints per residue	8.24
Number of long-range restraints per residue	1.79
Residual restraint violations	
Average number of distance violations per structure	
0.1–0.2 **Å**	40.65
0.2–0.5 **Å**	6.4
>0.5 **Å**	0.05 (max 0.5)
Average no. of dihedral angle violations per structure	
1–5°	3.75
>5°	1.3 (max 9.98°)

Model quality	
RMSD backbone atoms (Å), residues 81-113, 117-146	1.15 ± 0.17
RMSD heavy atoms (Å), residues 81-113, 117-146	1.82 ± 0.19
RMSD backbone atoms (Å), residues 698-710	0.74 ± 0.20
RMSD heavy atoms (Å), residues 698-710	1.84 ± 0.34
RMSD backbone atoms (Å), residues 2-39, 43-77	2.08 ± 0.51
RMSD heavy atoms (Å), residues 2-39, 43-77	2.64 ± 0.51
RMSD bond lengths (Å)	0.035
RMSD bond angles (°)	0.497
Ramachandran statistics res 1-148, 700-708	
Core (%)	96.7%
Allowed (%)	3.1%
Generous (%)	0.1%
Disallowed (%)	0.0%
Global quality scores (raw/Z score)	
WHATIF summary for the residues 1-148, 700-708	
Structure Z-scores	
1st generation packing quality	1.765 ± 0.706
2nd generation packing quality	4.507 ± 1.379
Ramachandran plot appearance	0.505 ± 0.324
Chi-1/Chi-2 rotamer normality	-0.084 ± 0.683
Backbone conformation	-0.787 ± 0.451
RMS Z-scores	
Bond lengths	1.218 ± 0.008
Bond angles	0.561 ± 0.008
Omega angle restraints	0.500 ± 0.038
Side chain planarity	0.956 ± 0.083
Improper dihedral distribution	0.811 ± 0.027
Inside/Outside distribution	1.000 ± 0.029
Model contents	
Ordered residue range	1-148, 700-708
Total no. of residues	218

Backbone dynamics of CaM:TRPV5$^{655-725}$

In order to study the dynamics of the CaM backbone in apo-state and in complex with TRPV5, we measured ^{15}N-T_1, ^{15}N-T_2 and ^{1}H-^{15}N heteronuclear NOE rates for the backbone amides for the native ^{15}N-CaM$_{WT}$, 1:1 ^{15}N-CaM$_{12}$:TRPV5$^{655-725}$ and 1:1 ^{15}N-CaM$_{WT}$:TRPV5$^{655-725}$ complexes. The sets of relaxation rates demonstrate significant differences between the three CaM species in the average values of the N- and C-lobes residues (See Fig. S5). Using the individual values of T_1 and T_2, we calculated residue-specific local correlation times $\tau_c(i)$ using the method suggested by Fushman et al.[37]. Fig. 5 displays histograms of these local $\tau_c(i)$ values, grouped by the N- and C-lobes for the three proteins. The individual lobes of CaM$_{WT}$ are expected to display an independent dynamic behaviour as result of the flexible residues in the central helix[57]. Indeed, the local τ_c values of each of the lobes of unbound CaM$_{WT}$ show a similar distribution around ~6.4 ns compatible with a protein domain of ~70 residues (Fig. 5A).

According to the structure and CSP data reported above, CaM$_{12}$ is engaged with TRPV5$^{655-725}$ using its C-lobe only. In agreement with this finding, its C-lobe τ_c value distribution is shifted to ~9.8 ns (Fig. 5B), arguably due to the increased mass and anisotropy, whereas the N-lobe shows a different and much smaller increase to ~8 ns. Presumably, this increase from 6.4 ns is caused by the increased drag exerted by the C-lobe now bound to the extensive TRPV5$^{655-725}$ moiety. The results, however, clearly indicate an independent dynamical behaviour of the two lobes in agreement with the absence of domain tethering. In contrast, the 1:1 CaM$_{WT}$:TRPV5$^{655-725}$ complex is expected to behave as one, tightly bound species and indeed, its N- and C-lobe τ_c value distributions (Fig. 5C) are now both similar and higher when compared to either native CaM or the 1:1 CaM$_{12}$:TRPV5$^{655-725}$ complex and correspond to the motion of a monomeric molecule with an effective mass of ~20 kDa.

In order to assess the dynamics of the TRPV5 moiety of the complex with CaM$_{12}$, we also measured the relaxation rates for the 1:1 ^{15}N-TRPV5$^{655-725}$:^{15}N-CaM$_{12}$ sample. For the fifteen distinct assigned amide nitrogen atoms of TRPV5$^{655-725}$, the values of local correlation times were obtained (Fig. S5C). Noticeably, a distinct group of residues, either within the TRPV5 helix or predicted to be α-helical (Q706,

N707, T708, L709, G710, L716 and N717), have an average τ_c value of 9.8 ns, close to the average τ_c values for CaM_{12} C-lobe bound to $TRPV5^{655-725}$. In contrast, residues from the regions predicted to be intrinsically disordered, exhibited a dramatic increase in their T_2 values, and hence a lower τ_c, values, demonstrating a high level of mobility in the C-terminal region of TRPV5.

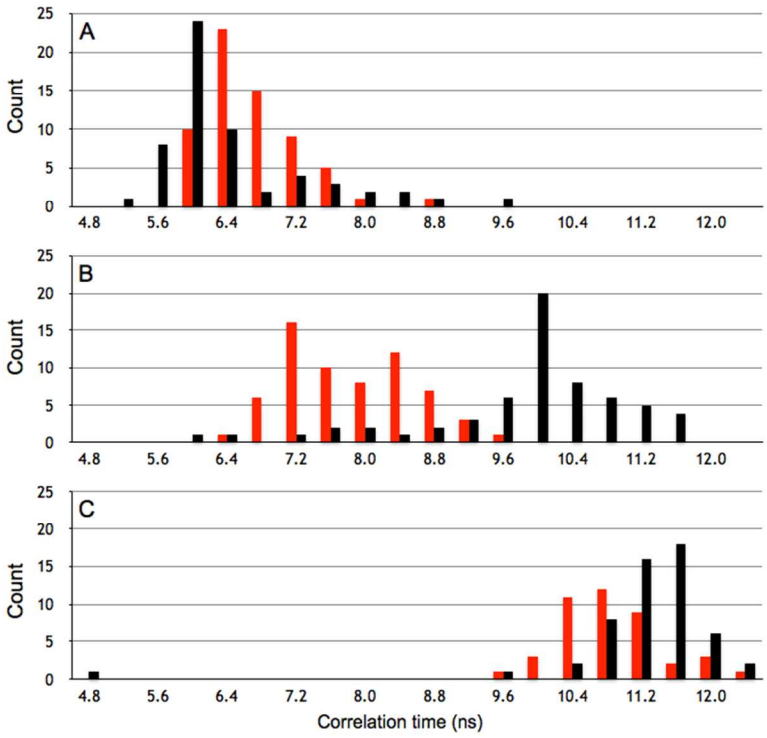

Figure 5. Dynamics of free CaM and CaM:$TRPV5^{655-725}$ complexes. Histograms of the distributions of the local correlation time values, $\tau_c(i)$ for N-lobe residues (red) and C-lobe residues (black) for (**A**) free CaM_{WT}, (**B**) 1:1 CaM_{12}:$TRPV5^{655-725}$ and (**C**) 1:1 CaM_{WT}:$TRPV5^{655-725}$.

Discussion

Our current study dissects the interaction between the TRPV5 C-terminus and CaM, thus identifying the tethering of CaM C-domain to TRPV5 monomer as a structural determinant of this interaction under low Ca^{2+}-conditions. The interaction between either TRPV5, or the closely related TRPV6, and CaM has been

studied previously, both *in vitro* and in a cellular context[11,13,54,58]. Functionally similar CaM binding sites have also been identified in the vanilloid family members TRPV1 [59] and TRPV4 [60], suggesting a common regulatory mechanism.

In the recently published crystal structure of CaM in complex with the conserved C-terminal TRPV1 region, CaM forms a 1:1 complex with a canonical compact conformation, wrapping around the α-helical TRPV1 C-terminus peptide using both N- and C-lobes[53]. Surprisingly, previous ^{15}N-HSQC analyses of the ^{15}N-CaM chemical shift differences upon titration with a short C-terminal TRPV5 peptide, already revealed a non-canonical mode of interaction between the peptide and CaM, with an unusual 1:2 stoichiometry and more prominent effects observed for the CaM C-lobe[3]. These findings were also confirmed by ITC measurements and observed for the paralogue TRPV6 [27]. In this current study we confirmed this unusual mode of interaction for longer TRPV5 fragments, alleviating the possibility that these effects originated from the insufficient length of the peptides. In contrast with the earlier TRPV5 work, however, we find that additional residues outside the previously defined minimal binding motif play an important role, affecting the patterns of interaction with CaM, as observed via NMR spectroscopy.

Our current studies also identify the tethering of the CaM C-lobe to the TRPV5 C-terminus as a crucial binding interaction. Indeed, the CSP values of the CaM C-lobe residues upon titration of TRPV5 are dramatically higher than those observed for the N-lobe residues and are nearly identical for both the wild-type CaM and the mutant CaM_{12}. As the latter is unable to bind Ca^{2+} by its N-lobe, we concluded that the CaM C-lobe, loaded with Ca^{2+} even at basal intracellular Ca^{2+} levels, mediates the interaction between TRPV5 and CaM (Fig 1, Fig. S2). Crucially, we established that ^{1}H-^{15}N-NMR spectra of CaM purified under Ca^{2+}-free conditions in complex with $TRPV5^{655-725}$ showed highly similar positioning of its C-lobe cross-peaks, indicative of the same structural arrangement as observed for the CaM_{WT} and CaM_{12} complexes, whereas most of its N-lobe cross-peaks were either shifted or even had disappeared altogether.

To establish the molecular basis of the CaM_{12}:TRPV5 complex, we solved its high-resolution solution structure and identified the key intermolecular interactions

that define the complex (Fig. 4). Our results show that CaM_{12} interacts with a short α-helical region of $TRPV5^{700-710}$ exclusively by its C-lobe. The key hydrophobic TRPV5 residues Trp701, Leu704 and Thr708 are anchored in the hydrophobic pocket in the CaM C-lobe.

Our structural findings are in agreement with a previous functional study, where the crucial role of Trp701, as well as Leu704, for CaM binding were demonstrated[54]. This study also reported that mutation of Arg705 led to diminished CaM binding and inhibited Ca^{2+}-dependent inactivation of TRPV5. In our structure, the aliphatic part of the Arg705 side-chain is located in a groove between the side-chains of CaM_{12} Met144 and Met145, which both demonstrate very large chemical shift changes upon $TRPV5^{655-725}$ binding. Our data suggest that it might be the binding affinity exerted by these Arg705-sidechain mediated interactions, rather than its charge, that are responsible for the effects of the mutation. Alternatively, an Arg705 mutation could affect the interactions with the N-lobe that ultimately result in formation of the 1:2 complex, crucial to the model of Bate et al.[27] (*vide infra*).

Functional studies also showed that mutation of Thr708 to aspartate leads to diminished CaM binding and loss of Ca^{2+}-induced CaM-dependent channel inactivation in HEK293 cells, and suggested that Thr708 is the target for parathyroid hormone-mediated phosphorylation of TRPV5 [12,54]. Our structure suggests that phosphorylation of Thr708 would not need to abrogate binding to the CaM C-lobe. Indeed NMR titrations using peptides with either a phosphomimetic T708D mutation, or a phosphorylated T708 residue are capable of binding CaM_{WT} (data not shown). As was the case for Arg705, we again speculate that N-lobe interaction required for 1:2 complex formation leading to channel inactivation may explain the *in vivo* observed effects.

CaM displays a remarkable variability in its interactions with target sequences[61]. The positioning of the Trp-X-X-Leu-Arg-X-X-Thr CaM-C-lobe interacting residues in TRPV5 constitutes a short, high-affinity CaM-binding motif, which appears to be a shorter variation of the previously described 1-5-8-14 CaM-binding motif[55]. In the structure of the CaM12:TRPV5 complex, the 14^{th} residue, i.e. Leu714, is clearly unstructured and does not display any interaction with the N-

lobe. It remains to be seen what role Leu714 would exert in the high-Ca^{2+} CaM:TRPV5 complex. However, Leu712 would be most similar to the crucial TRPV6 Leucine in the model of Bate et al.[27].

The non-canonical Trp-X-X-Leu motif is also present in the solution structures of CaM in complex with a Munc1 peptide[55] and the HIV-1 Matrix protein[56]. Both these complexes adopt an extended conformation with a modular architecture where the N- and C-lobes of CaM interact with short, but distinct helical regions of the protein, linked by unstructured linker regions. C- or N-lobe only modes of interaction of CaM with a target peptide were also demonstrated for numerous other channels regulated by CaM, notably the voltage-gated Ca^{2+}-channels[62], voltage-gated Na^{+}-channels[63], small conductance calcium-activated potassium channels[64], and aquaporins[65].

Our NMR relaxation studies of the unbound CaM_{wt}, CaM_{wt}:$TRPV5^{655-725}$ and CaM_{12}:$TRPV5^{655-725}$ complexes showed independent dynamic behaviour of the two lobes for both these complexes and support the absence of domain tethering in the latter complex (Fig. 5). The increased correlation times for the CaM_{wt}:$TRPV5^{655-725}$ complex, when compared to the unbound CaM_{wt} and CaM_{12}:$TRPV5^{655-725}$, confirm the formation of a single complex for the wild-type, involving both lobes in the interaction.

Altogether, our results establish a coordinating and crucial role of the CaM C-lobe in the formation of a high-affinity complex with the TRPV5 C-terminus under low-Ca^{2+} conditions. It is tempting to speculate that CaM could be pre-bound to the TRPV5 intracellular C-terminus *in vivo* when the channel is an active state. At first glance, this idea appears to be in disagreement with a previous cellular study that implied a dynamic association between CaM and the related TRPV6 channel[66]. However, the latter study used a CaM_{1234} mutant, defunct in Ca^{2+} binding for both the N- and C-lobes, rather than the CaM_{12} mutant used in our study. As also observed for the TRPV6 C-tail[27], CaM_{1234} abrogates all interaction with the TRPV5 C-tail as probed by our gel-filtration assays (Fig. S3). A pre-association between CaM

and an intracellular channel terminus has previously also been postulated for the SK channels[64], P/Q-type calcium channels[67] and voltage-gated sodium channels[68].

The TRPV5 C-tail is predicted and proven to be partially unstructured (Fig. S4) and the fragment used in this study is absent in the X-ray and EM structures of TRPV5, TRPV6, TRPV2 and TRPV1. We envision that the inherent flexibility is essential for the formation of the 1:2 CaM:TRPV5 complex as postulated by the model of Bate et al.[27], where the bridging of two TRPV5 tails by CaM leads to channel inactivation. Interestingly, TRPV5 is capable of functioning as hetero-tetramer with TRPV6, suggesting that the C-tail behaviour should be similar. Indeed, TRPV6 has similarly unstructured regions and the 1-4-8 CaM C-lobe interaction motif is conserved between the two channels.

In conclusion, we propose our CaM_{12}:$TRPV5^{655-725}$ structure as a representative for the low-calcium state of the novel three-state model for Ca^{2+}/CaM-dependent inactivation of TRPV channels, as recently proposed by Bate et al.[27]. In accordance with this model, we postulate that Ca^{2+} binding sites to the CaM N-lobe in response to elevated Ca^{2+}-concentrations, effectively serves as the channel's Ca^{2+} sensor. The Ca^{2+}-loaded N-lobe can subsequently mediate the additional interactions, leading to engagement of the N-lobe across two channel tails and ultimately resulting in its inactivation.

Accession numbers

The chemical shifts and restraints were submitted to the BMRB (accession no. **34161**) and the ensemble of 20 conformers to the wwPDB (accession no. **5OEO**).

Acknowledgements

We thank Dr. Fred Muskett for expert support and maintenance of our NMR equipment. GWV acknowledges funding during various stages of this project by the Dutch Organization of Scientific Research (NWO; grants 700.55.443 and 700.57.101), BBSRC (grant BB/J007897/1) and MRC (grants MR/L000555/1 and MR/P00038X/1). We thank Dr. Skinner for his assistance with the initial setup of the CcpNmr Analysis CYANA pipeline. We thank Tessa Vuister for her help in editing and formatting of the manuscript.

Supplementary materials

Five Figures and six Tables: ^{15}N-HSQC spectra of short and long TRPV5 constructs; ^{15}N-HSQC spectra of CaM_E and CaM_E:TRPV5 complexes under varying conditions; Assignments and mobility plots; ^{15}N-relaxtion data of CaM and TRPV5$^{655-725}$ as function of residue; gelshift essays assessing the binding of CaM_{WT}, CaM_{1234}, CaM_{12}, and CaM_{34} to the TRPV5$^{655-725}$ fragment and six Tables with key experimental NMR parameters.

References

(1) van de Graaf, S. F. J., Hoenderop, J. G. J., Gkika, D., Lamers, D., Prenen, J., Rescher, U., Gerke, V., Staub, O., Nilius, B., and Bindels, R. J. M. (2003) Functional expression of the epithelial Ca2+ channels (TRPV5 and TRPV6) requires association of the S100A10–annexin 2 complex. *EMBO J 22*, 1478–1487.

(2) Frick, K. K., and Bushinsky, D. A. (2003) Molecular mechanisms of primary hypercalciuria. *J Am Soc Nephrol 14*, 1082–1095.

(3) Hoenderop, J. G. J., van Leeuwen, J. P. T. M., van der Eerden, B. C. J., Kersten, F. F. J., van derKemp, A. W. C. M., Mérillat, A.-M., Waarsing, J. H., Rossier, B. C., Vallon, V., Hummler, E., and Bindels, R. J. M. (2003) Renal Ca2+ wasting, hyperabsorption, and reduced bone thickness in mice lacking TRPV5. *Journal of Clinical Investigation 112*, 1906–1914.

(4) van Abel, M., Hoenderop, J. G. J., Dardenne, O., St Arnaud, R., van Os, C. H., van Leeuwen, H. J. P. T. M., and Bindels, R. J. M. (2002) 1,25-dihydroxyvitamin D(3)-independent stimulatory effect of estrogen on the expression of ECaC1 in the kidney. *J Am Soc Nephrol 13*, 2102–2109.

(5) Chang, Q., Hoefs, S., van der Kemp, A. W., Topala, C. N., Bindels, R. J., and Hoenderop, J. G. J. (2005) The ß-Glucuronidase Klotho Hydrolyzes and Activates the TRPV5 Channel. *Science 310*, 490–493.

(6) Zhang, W., Na, T., and Peng, J.-B. (2009) Nedd4-2 and Nedd4 mediate degradation of TRPV6 and TRPV5. *The FASEB Journal 23*, 998.16–998.16.

(7) Vennekens, R., Hoenderop, J., Prenen, J., Stuiver, M., Willems, P., Droogmans, G., Nilius, B., and Bindels, R. (2000) Permeation and gating properties of the novel epithelial Ca2+ channel. *J Biol Chem 275*, 3963–3969.

(8) Nilius, B., Prenen, J., Vennekens, R., Hoenderop, J. G. J., Bindels, R. J. M., and Droogmans, G. (2001) Modulation of the epithelial calcium channel, ECaC, by intracellular Ca2. *Cell Calcium 29*, 417–428.

(9) Lambers, T. T., Mahieu, F., Oancea, E., Hoofd, L., de Lange, F., Mensenkamp, A. R., Voets, T., Nilius, B., Clapham, D. E., Hoenderop, J. G. J., and Bindels, R. J. (2006) Calbindin-D-28K dynamically controls TRPV5-mediated Ca2+ transport. *Embo Journal 25*, 2978–2988.

(10) Gkika, D., Mahieu, F., Nilius, B., Hoenderop, J. G. J., and Bindels, R. J. M. (2004) 80K-H as a New Ca2+ Sensor Regulating the Activity of the Epithelial Ca2+ Channel Transient Receptor Potential Cation Channel V5 (TRPV5). *Journal of Biological Chemistry 279*, 26351–26357.

(11) Lambers, T., Weidema, A., Nilius, B., Hoenderop, J. G. J., and Bindels, R. (2004) Regulation of the Mouse Epithelial Ca2+ Channel TRPV6 by the Ca2+-sensor Calmodulin. *Journal of Biological Chemistry 279*, 28855.

(12) de Groot, T., Lee, K., Langeslag, M., Xi, Q., Jalink, K., Bindels, R. J. M., and Hoenderop, J. G. J. (2009) Parathyroid hormone activates TRPV5 via PKA-dependent phosphorylation. *Journal of the American Society of Nephrology 20*, 1693–1704.

(13) Kovalevskaya, N. V., Bokhovchuk, F. M., and Vuister, G. W. (2012) The TRPV5/6 calcium channels contain multiple calmodulin binding sites with differential binding properties. *J. Struct. Funct. Genomics 13*, 91–100.

(14) Babu, Y. S., Sack, J. S., Greenhough, T. J., Bugg, C. E., Means, A. R., and Cook,

W. J. (1985) Three-dimensional structure of calmodulin. *Nature 315*, 37–40.
(15) Babu, Y. S., Bugg, C. E., and Cook, W. J. (1988) Structure of calmodulin refined at 2.2 A resolution. *J. Mol. Biol. 204*, 191–204.
(16) Nilius, B., Weidema, F., Prenen, J., Hoenderop, J. G. J., Vennekens, R., Hoefs, S., Droogmans, G., and Bindels, R. J. (2003) The carboxyl terminus of the epithelial Ca2+ channel ECaC1 is involved in Ca2+-dependent inactivation. *Pflugers Arch 445*, 584–588.
(17) Cao, C., Zakharian, E., Borbiro, I., and Rohacs, T. (2013) Interplay between Calmodulin and Phosphatidylinositol 4,5-Bisphosphate in Ca2+-induced Inactivation of Transient Receptor Potential Vanilloid 6 Channels. *Journal of Biological Chemistry 288*, 5278–5290.
(18) Singh, B. B., Liu, X., Tang, J., Zhu, M. X., and Ambudkar, I. S. (2002) Calmodulin Regulates Ca2+-Dependent Feedback Inhibition of Store-Operated Ca2+ Influx by Interaction with a Site in the C Terminus of TrpC1. *Mol Cell 9*, 739–750.
(19) Numazaki, M., Tominaga, T., Takeuchi, K., Murayama, N., Toyooka, H., and Tominaga, M. (2003) Structural determinant of TRPV1 desensitization interacts with calmodulin. *Proc. Natl. Acad. Sci. U.S.A. 100*, 8002–8006.
(20) Strotmann, R., Schultz, G., and Plant, T. D. (2003) Ca2+-dependent Potentiation of the Nonselective Cation Channel TRPV4 Is Mediated by a C-terminal Calmodulin Binding Site. *Journal of Biological Chemistry 278*, 26541–26549.
(21) Mercado, J., Gordon-Shaag, A., Zagotta, W. N., and Gordon, S. E. Ca2+-Dependent Desensitization of TRPV2 Channels Is Mediated by Hydrolysis of Phosphatidylinositol 4,5-Bisphosphate. *jneurosci.org*.
(22) Liao, M., Cao, E., Julius, D., and Cheng, Y. (2013) Structure of the TRPV1 ion channel determined by electron cryo-microscopy. *Nature 504*, 107–112.
(23) Zubcevic, L., Herzik, M. A., Chung, B. C., Liu, Z., Lander, G. C., and Lee, S.-Y. (2016) Cryo-electron microscopy structure of the TRPV2 ion channel. *Nat Struct Mol Biol 23*, 180–186.
(24) Hughes, T. E. T., Lodowski, D. T., Huynh, K. W., Yazici, A., Del Rosario, J., Kapoor, A., Basak, S., Samanta, A., Han, X., Chakrapani, S., Zhou, Z. H., Filizola, M., Rohacs, T., Han, S., and Moiseenkova-Bell, V. Y. (2018) Structural basis of TRPV5 channel inhibition by econazole revealed by cryo-EM. *Nat Struct Mol Biol* 1–12.
(25) Saotome, K., Singh, A. K., Yelshanskaya, M. V., and Sobolevsky, A. I. (2016) Crystal structure of the epithelial calcium channel TRPV6. *Nature 534*, 506–511.
(26) McGoldrick, L. L., Singh, A. K., Saotome, K., Yelshanskaya, M. V., Twomey, E. C., Grassucci, R. A., and Sobolevsky, A. I. (2018) Opening of the human epithelial calcium channel TRPV6. *Nature 553*, 233–237.
(27) Bate, N., Caves, R. E., Skinner, S. P., Goult, B. T., Basran, J., Mitcheson, J. S., and Vuister, G. W. (2018) A Novel Mechanism for Calmodulin Dependent Inactivation of Transient Receptor Potential Vanilloid 6. *Biochemistry 57*, DOI:10.1021/acs.biochem.7b01286.
(28) Wu, P.-R., Kuo, C.-C., Yet, S.-F., Liou, J.-Y., Wu, K. K., and Chen, P.-F. (2012) Lobe-Specific Calcium Binding in Calmodulin Regulates Endothelial Nitric Oxide Synthase Activation. *PLoS ONE 7*, e39851.
(29) Delaglio, F., Grzesiek, S., Vuister, G. W., Zhu, G., Pfeifer, J., and Bax, A. (1995)

NMRPipe: a multidimensional spectral processing system based on UNIX pipes. *J Biomol NMR 6*, 277–293.

(30) Vranken, W. F., Boucher, W., Stevens, T. J., Fogh, R. H., Pajon, A., Llinás, M., Ulrich, E. L., Markley, J. L., Ionides, J., and Laue, E. D. (2005) The CCPN data model for NMR spectroscopy: development of a software pipeline. *Proteins 59*, 687–696.

(31) Skinner, S. P., Fogh, R. H., Boucher, W., Ragan, T. J., Mureddu, L. G., and Vuister, G. W. (2016) CcpNmr AnalysisAssign: a flexible platform for integrated NMR analysis. *J Biomol NMR 66*, 111–124.

(32) Hyberts, S. G., Milbradt, A. G., Wagner, A. B., Arthanari, H., and Wagner, G. (2012) Application of iterative soft thresholding for fast reconstruction of NMR data non-uniformly sampled with multidimensional Poisson Gap scheduling. *J Biomol NMR 52*, 315–327.

(33) Bermel, W., Bertini, I., Duma, L., Felli, I. C., Emsley, L., Pierattelli, R., and Vasos, P. R. (2005) Complete assignment of heteronuclear protein resonances by protonless NMR spectroscopy. *Angew Chem Int Ed Engl 44*, 3089–3092.

(34) Bermel, W., Bertini, I., Felli, I., Piccioli, M., and Pierattelli, R. (2006) 13C-detected protonless NMR spectroscopy of proteins in solution. *Prog Nucl Mag Res Sp 48*, 25–45.

(35) Bax, A., Clore, G. M., and Gronenborn, A. M. (1990) 1H-1H Correlation via Isotropic Mixing of 13C Magnetization, a New Three-Dimensional Approach for Assigning 1H and 13C Spectra of 13C-Enriched Proteins. *Journal of Magnetic Resonance 88*, 425–431.

(36) Yamazaki, T., Forman-Kay, J. D., and Kay, L. E. (1993) Two-dimensional NMR experiments for correlating carbon-13.beta. and proton.delta./.epsilon. chemical shifts of aromatic residues in 13C-labeled proteins via scalar couplings. *J Am Chem Soc 115*, 11054–11055.

(37) Fushman, D., Weisemann, R., Thuring, H., and Rüterjans, H. (1994) Determination of the backbone mobility of ribonuclease T1 and its 2'GMP complex using molecular dynamics simulations and NMR relaxation data *4*, 61–78.

(38) Güntert, P. (2009) Automated structure determination from NMR spectra. *Eur Biophys J 38*, 129–143.

(39) Skinner, S. P., Goult, B. T., Fogh, R. H., Boucher, W., Stevens, T. J., Laue, E. D., and Vuister, G. W. (2015) Structure calculation, refinement and validation using CcpNmr Analysis. *Acta Crystallogr D Biol Crystallogr 71*, 154–161.

(40) Shen, Y., Delaglio, F., Cornilescu, G., and Bax, A. (2009) TALOS+: a hybrid method for predicting protein backbone torsion angles from NMR chemical shifts. *J Biomol NMR 44*, 213–223.

(41) Cheung, M.-S., Maguire, M. L., Stevens, T. J., and Broadhurst, R. W. (2010) DANGLE: A Bayesian inferential method for predicting protein backbone dihedral angles and secondary structure. *Journal of Magnetic Resonance 202*, 223–233.

(42) Doreleijers, J. F., Sousa da Silva, A. W., Krieger, E., Nabuurs, S. B., Spronk, C. A. E. M., Stevens, T. J., Vranken, W. F., Vriend, G., and Vuister, G. W. (2012) CING: an integrated residue-based structure validation program suite. *J Biomol NMR 54*, 267–283.

(43) Krieger, E., and Vriend, G. (2014) YASARA View—molecular graphics for all

devices—from smartphones to workstations. *Bioinformatics 30*, 2981–2982.
(44) Bardiaux, B., Malliavin, T., and Nilges, M. (2012) ARIA for Solution and Solid-State NMR, in *Protein NMR Techniques*, pp 453–483. Humana Press, Totowa, NJ.
(45) Rieping, W., Habeck, M., and Nilges, M. (2005) Modeling errors in NOE data with a log-normal distribution improves the quality of NMR structures. *J Am Chem Soc 127*, 16026–16027.
(46) Montelione, G. T., Nilges, M., Bax, A., Güntert, P., Herrmann, T., Richardson, J. S., Schwieters, C. D., Vranken, W. F., Vuister, G. W., Wishart, D. S., Berman, H. M., Kleywegt, G. J., and Markley, J. L. (2013) Recommendations of the wwPDB NMR Validation Task Force. *Structure 21*, 1563–1570.
(47) Kovalevskaya, N. V., Schilderink, N., and Vuister, G. W. (2011) Expression and purification of the C-terminal fragments of TRPV5/6 channels. *Protein Expression and Purification 80*, 28–33.
(48) Linse, S., Helmersson, A., and Forsen, S. (1991) Calcium-Binding to Calmodulin and Its Globular Domains. *J Biol Chem 266*, 8050–8054.
(49) Bonventre, J. V., and Cheung, J. Y. (1986) Cytosolic Free Calcium-Concentration in Cultured Renal Epithelial-Cells. *American Journal of Physiology 250*, F329–F338.
(50) Gangola, P., and Rosen, B. P. (1987) Maintenance of Intracellular Calcium in *Escherichia Coli*. *J. Biol. Chem. 262*, 12570–12574.
(51) Ikura, M., Clore, G. M., Gronenborn, A., Zhu, G., Klee, C., and Bax, A. (1992) Solution structure of a calmodulin-target peptide complex by multidimensional NMR. *Science 256*, 632–638.
(52) Bin Xue, Dunbrack, R. L., Williams, R. W., Dunker, A. K., and Uversky, V. N. (2010) PONDR-FIT: A Meta-Predictor of Intrinsically Disordered Amino Acids. *Biochim Biophys Acta 1804*, 996–1010.
(53) Lau, S.-Y., Procko, E., and Gaudet, R. (2012) Distinct properties of Ca2+-calmodulin binding to N- and C-terminal regulatory regions of the TRPV1 channel. *J Gen Physiol 140*, 541–555.
(54) de Groot, T., Kovalevskaya, N. V., Verkaart, S., Schilderink, N., Felici, M., van der Hagen, E. A. E., Bindels, R. J. M., Vuister, G. W., and Hoenderop, J. G. (2011) Molecular Mechanisms of Calmodulin Action on TRPV5 and Modulation by Parathyroid Hormone. *Molecular and Cellular Biology 31*, 2845–2853.
(55) Rodriguez-Castañeda, F., Maestre-Martínez, M., Coudevylle, N., Dimova, K., Junge, H., Lipstein, N., Lee, D., Becker, S., Brose, N., Jahn, O., Carlomagno, T., and Griesinger, C. (2010) Modular architecture of Munc13/calmodulin complexes: dual regulation by Ca2+ and possible function in short-term synaptic plasticity. *Embo Journal 29*, 680–691.
(56) Vlach, J., Samal, A. B., and Saad, J. S. (2014) Solution Structure of Calmodulin Bound to the Binding Domain of the HIV-1 Matrix Protein. *J Biol Chem 289*, 8697–8705.
(57) Barbato, G., Ikura, M., Kay, L. E., Pastor, R. W., and Bax, A. (1992) Backbone dynamics of calmodulin studied by 15N relaxation using inverse detected two-dimensional NMR spectroscopy: the central helix is flexible. *Biochemistry 31*, 5269–5278.
(58) Niemeyer, B. A., Bergs, C., Wissenbach, U., Flockerzi, V., and Trost, C. (2001)

Competitive regulation of CaT-like-mediated Ca2+ entry by protein kinase C and calmodulin. *Proc Natl Acad Sci USA 98*, 3600–3605.

(59) Numazaki, M., Tominaga, T., Takeuchi, K., Murayama, N., Toyooka, H., and Tominaga, M. (2003) Structural determinant of TRPV1 desensitization interacts with calmodulin. *Proc Natl Acad Sci USA 100*, 8002–8006.

(60) Strotmann, R., Schultz, G., and Plant, T. D. (2003) Ca2+-dependent Potentiation of the Nonselective Cation Channel TRPV4 Is Mediated by a C-terminal Calmodulin Binding Site. *Journal of Biological Chemistry 278*, 26541–26549.

(61) Kovalevskaya, N. V., van de Waterbeemd, M., Bokhovchuk, F. M., Bate, N., Bindels, R. J. M., Hoenderop, J. G. J., and Vuister, G. W. (2013) Structural analysis of calmodulin binding to ion channels demonstrates the role of its plasticity in regulation. *Pflugers Arch 465*, 1507–1519.

(62) Kim, E. Y., Rumpf, C. H., Fujiwara, Y., Cooley, E. S., Van Petegem, F., and Minor, D. L., Jr. (2008) Structures of CaV2 Ca2+/CaM-IQ Domain Complexes Reveal Binding Modes that Underlie Calcium-Dependent Inactivation and Facilitation. *Structure 16*, 1455–1467.

(63) Chagot, B., and Chazin, W. J. (2011) Solution NMR structure of Apo-calmodulin in complex with the IQ motif of human cardiac sodium channel NaV1.5. *J. Mol. Biol. 406*, 106–119.

(64) Schumacher, M. A., Rivard, A. F., Bächinger, H. P., and Adelman, J. P. (2001) Structure of the gating domain of a Ca2|[plus]|-activated K|[plus]| channel complexed with Ca2|[plus]|/calmodulin. *Nature 410*, 1120–1124.

(65) Reichow, S. L., and Gonen, T. (2008) Noncanonical binding of calmodulin to aquaporin-0: implications for channel regulation. *Structure 16*, 1389–1398.

(66) Derler, I., Hofbauer, M., Kahr, H., Fritsch, R., Muik, M., Kepplinger, K., Hack, M. E., Moritz, S., Schindl, R., Groschner, K., and Romanin, C. (2006) Dynamic but not constitutive association of calmodulin with rat TRPV6 channels enables fine tuning of Ca2+-dependent inactivation. *J Physiol (Lond) 577*, 31–44.

(67) Lee, A., Scheuer, T., and Catterall, W. A. (2000) Ca2+/calmodulin-dependent facilitation and inactivation of P/Q-type Ca2+ channels. *J. Neurosci. 20*, 6830–6838.

(68) Sarhan, M. F., Tung, C.-C., Van Petegem, F., and Ahern, C. A. (2012) Crystallographic basis for calcium regulation of sodium channels. *Proc Natl Acad Sci USA 109*, 3558–3563.

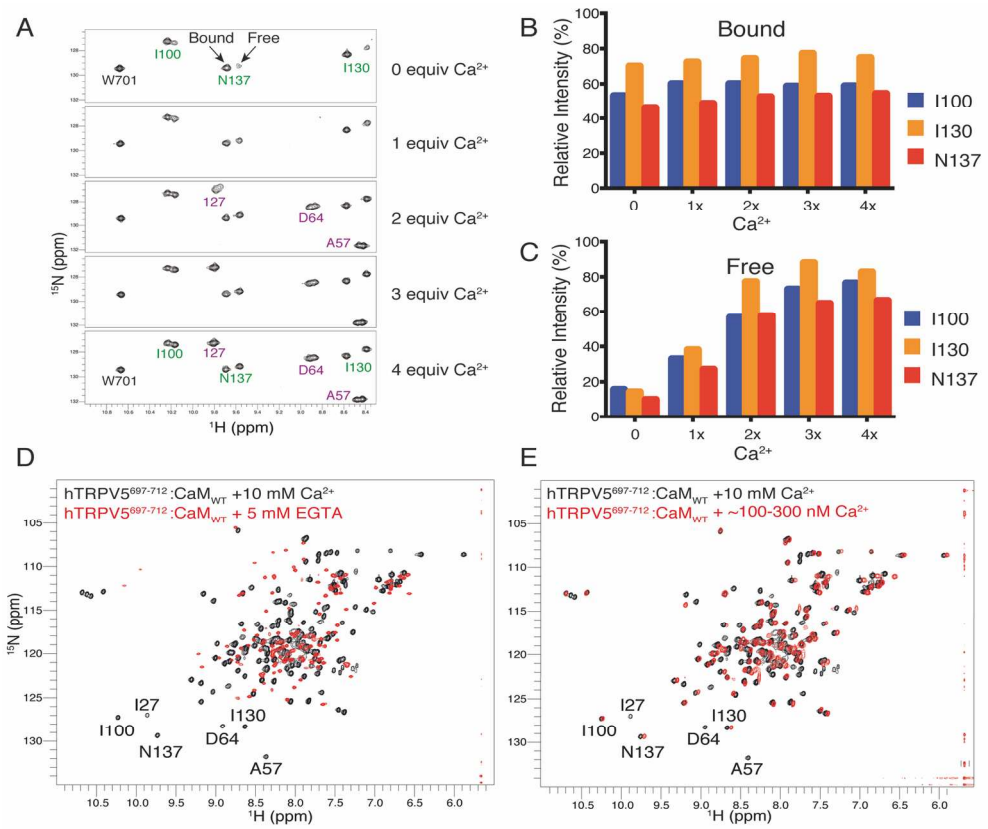

Figure 1

150x124mm (300 x 300 DPI)

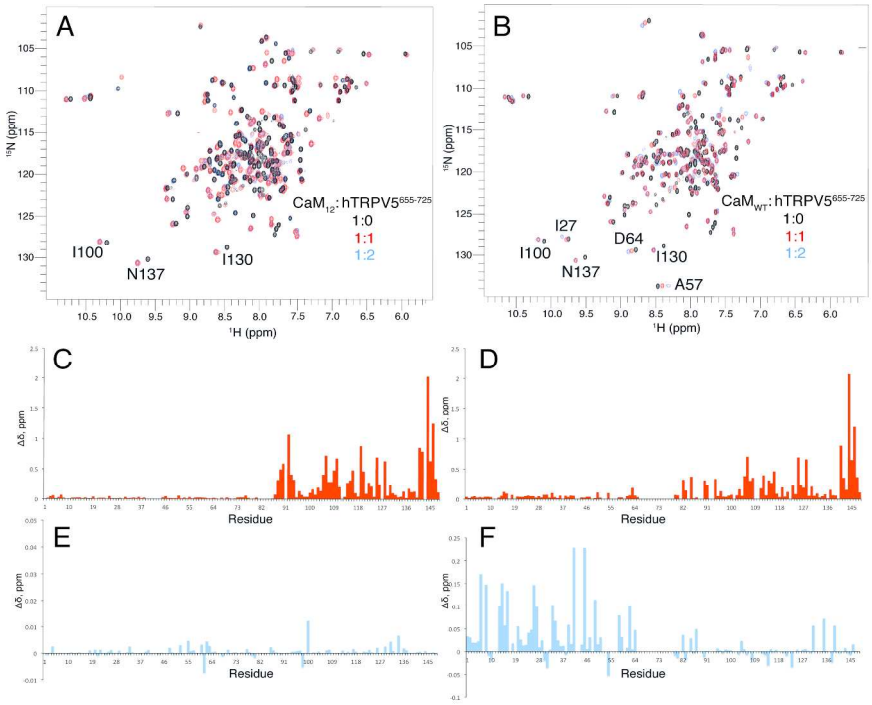

275x380mm (300 x 300 DPI)

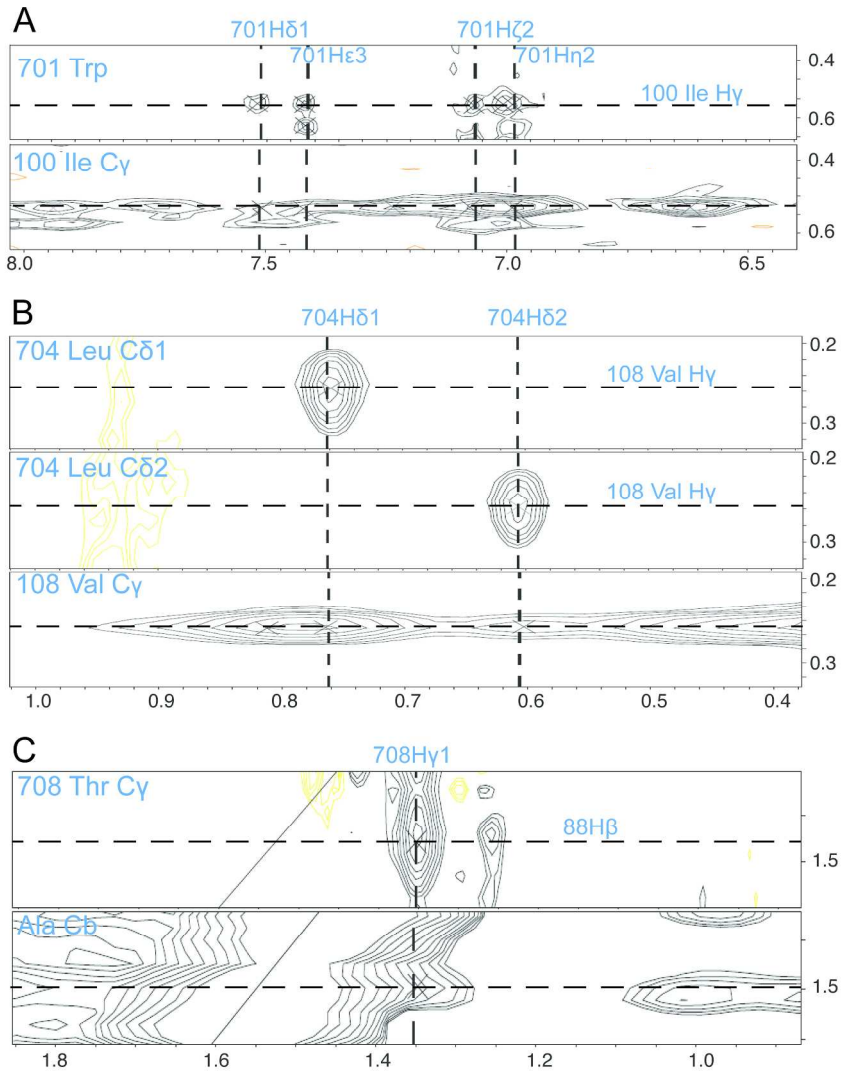

221x285mm (300 x 300 DPI)

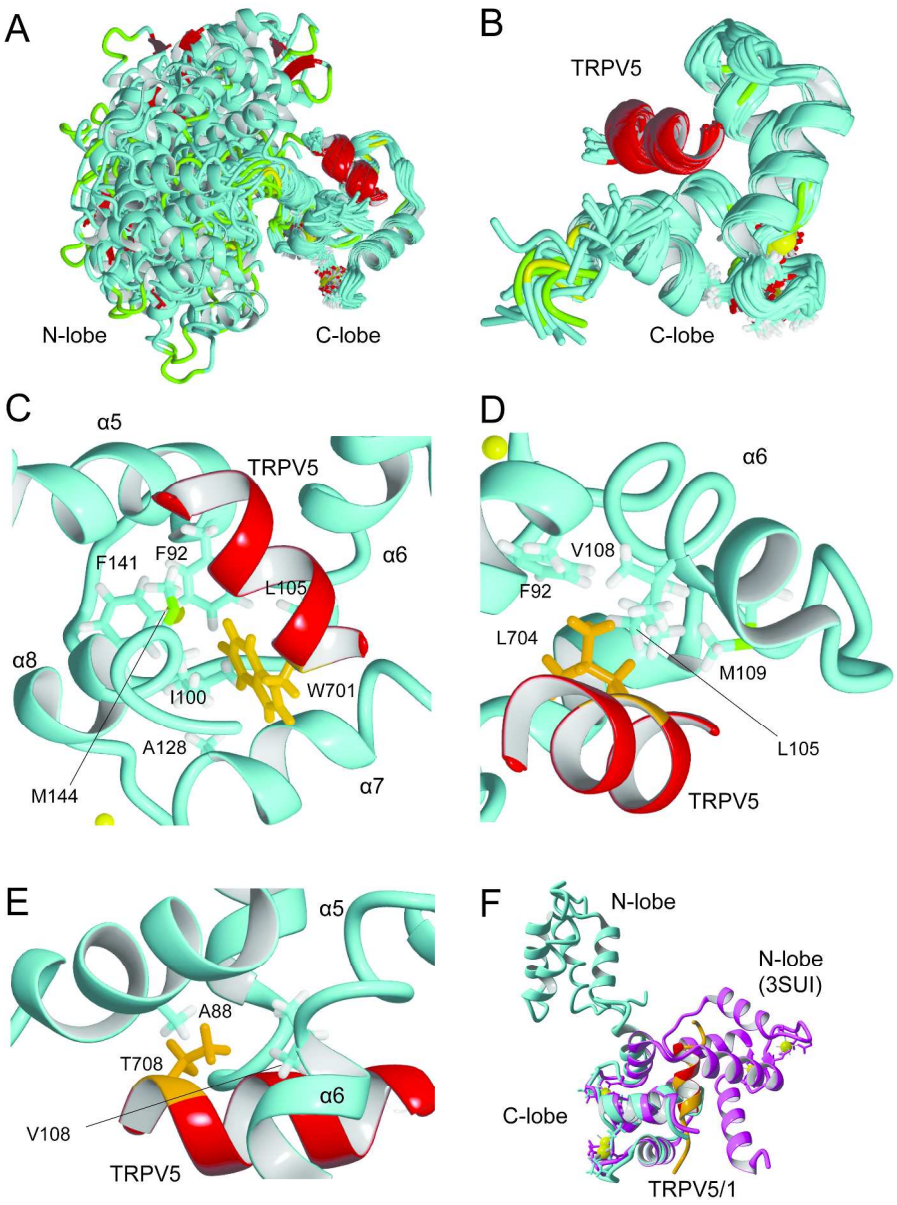

268x361mm (300 x 300 DPI)

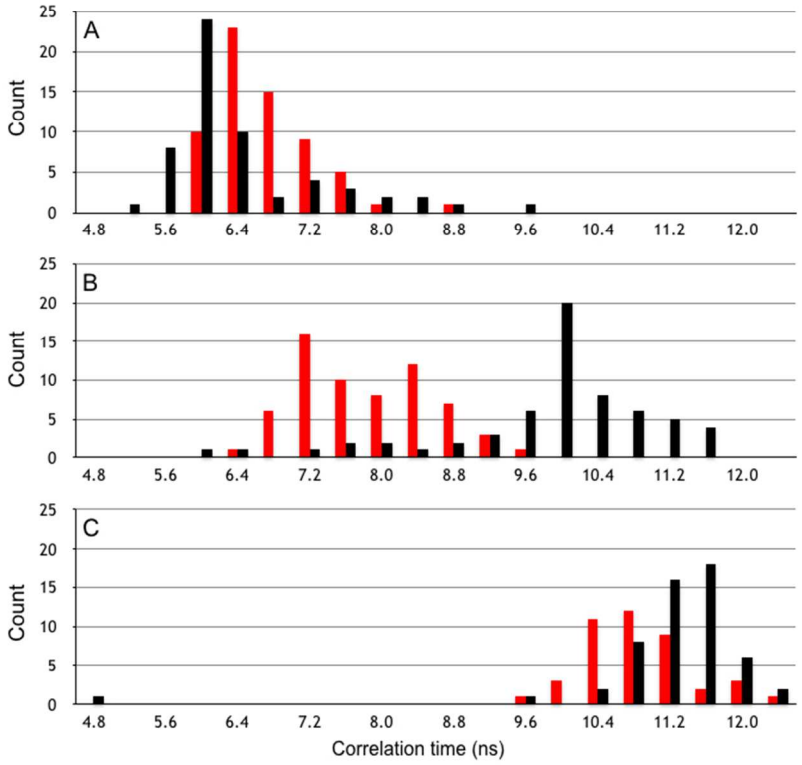

266x355mm (72 x 72 DPI)

For Table of Contents use only

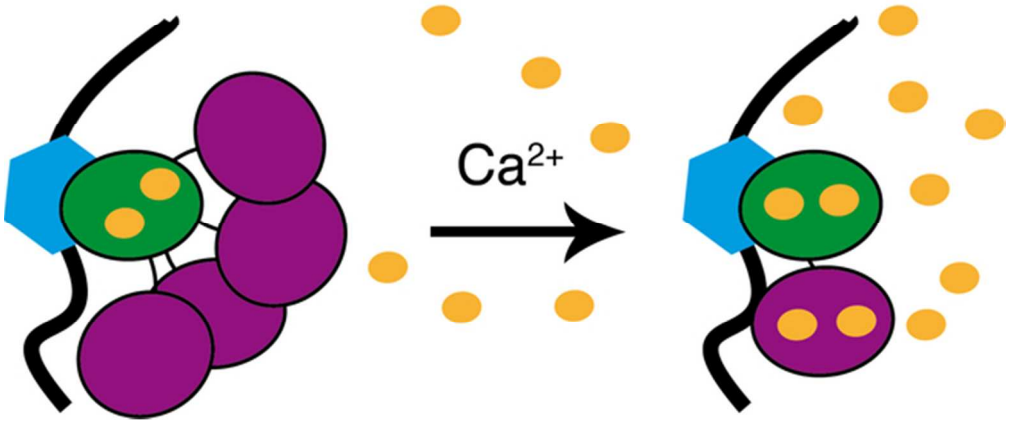

For Table of Contents only

55x38mm (300 x 300 DPI)